NANO LETTERS

pubs.acs.org/NanoLett

Letter

Two-Dimensional Electrically Conductive Metal–Organic Framework Boosts Synaptic Plasticity for Dynamic Image Refresh, Classification, and Efferent Neuromuscular Systems

Huanhuan Wei, Jiaqi Liu, Yao Ni, Xuanxin Hu, Xiuliang Lv, Lu Yang, Gang He, Zhipeng Xu, Jiangdong Gong, Chengpeng Jiang, Dawei Feng,* and Wentao Xu*

Cite This: *Nano Lett.* 2024, 24, 15379–15387

Read Online

ACCESS | Metrics & More | Article Recommendations | Supporting Information

ABSTRACT: We present a two-dimensional (2D) electrically conductive metal–organic framework (EC-MOF)-based artificial synapse. The intrinsic electronic conductivity and subnanometer channels of the EC-MOF facilitate efficient ion diffusion, enable a high density of active redox centers, and significantly enhance capacitance within the artificial synapse. As a result, the synapse operates at an ultralow voltage of 10 mV and exhibits a remarkably low power consumption of approximately 1 fW, along with the longest retention time recorded for two-terminal electrolyte-type artificial synapses to date. The alignment of the quantum size of the subnanometer pores in the EC-MOF with various cations allows for versatile synaptic plasticity. This capability is applied to image refresh, classification, and efferent signal transmission for controlling artificial muscles, thereby offering a methodology for achieving tunable neuromorphic properties. These findings suggest the potential application of metal–organic frameworks in artificial nervous systems for future brain-inspired computation, peripheral interfaces, and neurorobotics.

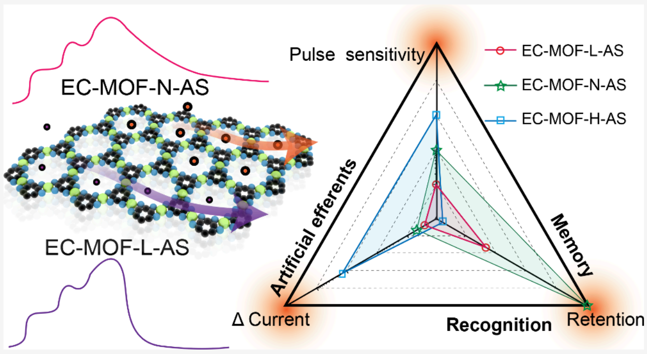

KEYWORDS: *artificial synapse, electrically conductive metal–organic framework, pseudocapacitance, synaptic plasticity, power consumption*

Nervous systems integrate sensory input from the peripheral nervous system with information processing by the central nervous system, delivering signals of plasticity changes through the synaptic cleft.[1−7] Ionic/electronic hybrid artificial synapses (ASs) have been developed to exploit ion modulation at the electrolyte/semiconductor interface under the action of pulses; these stimuli can modify the responses ("weights") of the devices in ways that emulate synaptic signal transmission.[8−12] Short-term plasticity in electrolyte-gate synaptic transistors can be achieved by electrostatic modulation, necessitating impermeable channel-layer materials, whereas long-term plasticity is realized via electrochemical doping,[13−18] requiring permeable channel-layer materials.

However, in electrolyte-type ASs, the retention of the plasticity is short, because ions form the dominant diffuse layer and compact layer at the interface of the semiconductor.[19−24] Considerable efforts have been made to boost synaptic retention by applying heavy ion doping into organic semiconductors of different crystallinity.[25−27] To extend the duration of plasticity change in electrolyte/semiconductor heterojunction devices, materials with excellent electrical conductivity, high density of hosting sites (redox active sites), as well as low ion diffusion barriers are highly desired.

Metal–organic frameworks (MOFs) consist of metal ions or clusters coordinated to organic ligands to form two-, or three-dimensional structures. Due to their synthetic tunability, diverse functionality and intrinsic porosity, MOFs have shown promising performances in catalysis, gas storage and separation, energy storage,[28−31] and environmental[32−34] and biomedical applications.[35−37] Recently, electrically conductive MOFs (EC-MOFs) have attracted growing attention for their excellent electrical conductivity and redox activity, which yield huge pseudocapacitance due to Faradaic process inside of the pores.[38−40] These features of EC-MOFs in artificial synapses (EC-MOF-ASs) to increase the variety of synaptic cleft plasticity change, holding promise for the development of advanced brain-like information processing and analysis capabilities.

Received: September 19, 2024
Revised: November 11, 2024
Accepted: November 13, 2024
Published: November 21, 2024

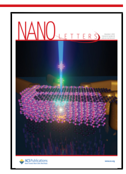

https://doi.org/10.1021/acs.nanolett.4c04650
Nano Lett. 2024, 24, 15379–15387

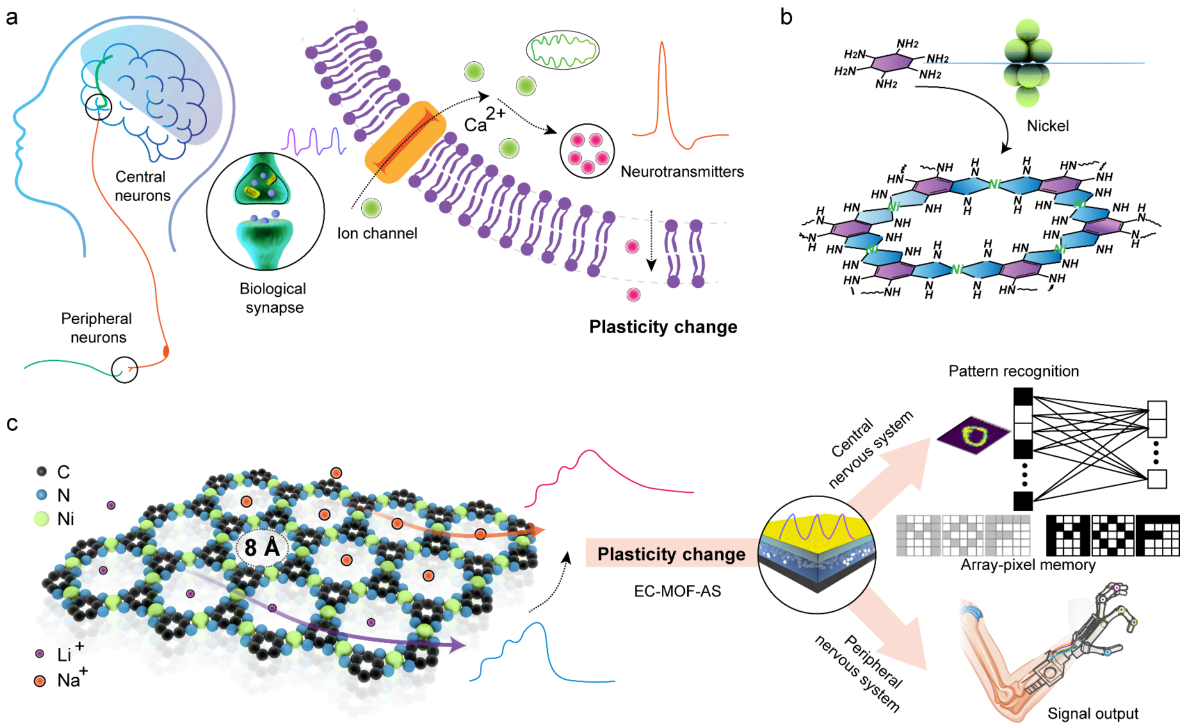

Figure 1. Schematic illustration of EC-MOF-ASs. a) Neurons in human brain and information transfer in biological synapse cleft. b) Schematic representation of the synthetic route for Ni-HAB. c) Plasticity modulation of EC-MOF-ASs.

Herein we present a junction-type EC-MOF-AS by coupling an EC-MOF film with electrolytes to achieve electrochemical plasticity, such as pulse-dependent changes in postsynaptic current. The long retention time (>30 min) and femtowatt power consumption are achieved. As proof-of-concept, the observed plasticity in neuromorphic devices is applied in array-pixel memory, pattern recognition and signal transduction, and in the development of artificial efferent nerves that regulate the motion of artificial muscles.

The synaptic cleft is the basic unit that connects sensory neurons, motor neurons, and interneurons that compose neural circuits (Figure 1a).[6,41] An arriving action potential initiates the release of neurotransmitters and the influx of calcium ions into the synaptic cleft.[42−44] Repeated stimuli can cause modifications to the responsiveness of the clefts. To emulate these responses, EC-MOFs can be engineered to enable plasticity alteration of responses to various ions at the electrolyte interface. Hexaaminobenzene (HAB)[45−51] is a small ligand that facilitates the construction of subnanopore EC-MOFs (8 Å) that include metal species such as Ni^{2+} (Figure 1b), and thereby enable regulation of the migration kinetics of various alkali metal ions (Figure 1c). In this work, vertical two-terminal electrolyte-type EC-MOF-ASs were fabricated by stacking EC-MOFs with various ionic electrolytes (Li^+, labeled as EC-MOF-L-AS; Na^+, labeled as EC-MOF-N-AS; and H^+, labeled as EC-MOF-H-AS; Supporting Information, Figure S1).

Both the powder and thin film products of Ni-based materials were prepared according to literature procedures (Supporting Information, Figure S2).[47] The particle size of the EC-MOF is about 50 nm, and transmission electron microscope (TEM), high-resolution TEM photographs and the corresponding high-resolution fast Fourier transform pattern show clear fringes (0.347 nm), which indicate that the crystallinity is good (Supporting Information, Figures S3 and S4). Atomic force microscopy (AFM) images of the surface of the as-prepared EC-MOF nanoparticle films show both surface average roughness R_a < 20 nm and root mean squared roughness <20 nm (Supporting Information, Figure S5). The presence of Ni and N on the surface of the films was confirmed by high-resolution X-ray photoelectron spectroscopy (XPS) spectra (Supporting Information, Figure S6). Current−voltage (I−V) curves of EC-MOF-L-AS were investigated to illustrate the kinetics of ions migration (Supporting Information, Figure S7). The response eventually stabilized and developed reversibility as the number of scanning turns increased; an apparent negative differential resistance (NDR) at low potential (1.5 to 1.8 V) is still discernible. The conspicuous NDR in EC-MOF/electrolyte system suggests a dominant pseudocapacitive mechanism and a doping/dedoping kinetic process of ions at the interface under periodic electric fields.[52]

EC-MOF-L-AS undergoes a process analogous to information transmission across a biological synaptic cleft (Figure 2). As the amplitude (ranging from 0.5 to 5 V) and width (from 1.5 to 5 s) of the presynaptic pulse fluctuate continuously, the postsynaptic current modulates in response to changes in pulse (Figure 2a). An intriguing phenomenon is observed at a threshold of approximately 15 pA for changes in postsynaptic currents with increasing pulse amplitude, which may be attributed to steric blockage of ions entering the EC-MOF. The current retention time for each pulse width (1.5, 2.2, 2.9, 3.6, 4.3, 5.0 s) increased following continuous pulse excitation at various amplitudes (Supporting Information, Figure S8). Notably, the current did not return to its initial level after a decay period of 1 min from the peak. The relaxation-time constant τ of the decay curves was 11 ± 1 s, derived from fitting the data to a one-phase exponential decay function.[53] Under sequential excitation by two identical pulses (3 V, 1.5 s), two sequential current peaks with distinct magnitudes (first

https://doi.org/10.1021/acs.nanolett.4c04650
Nano Lett. 2024, 24, 15379−15387

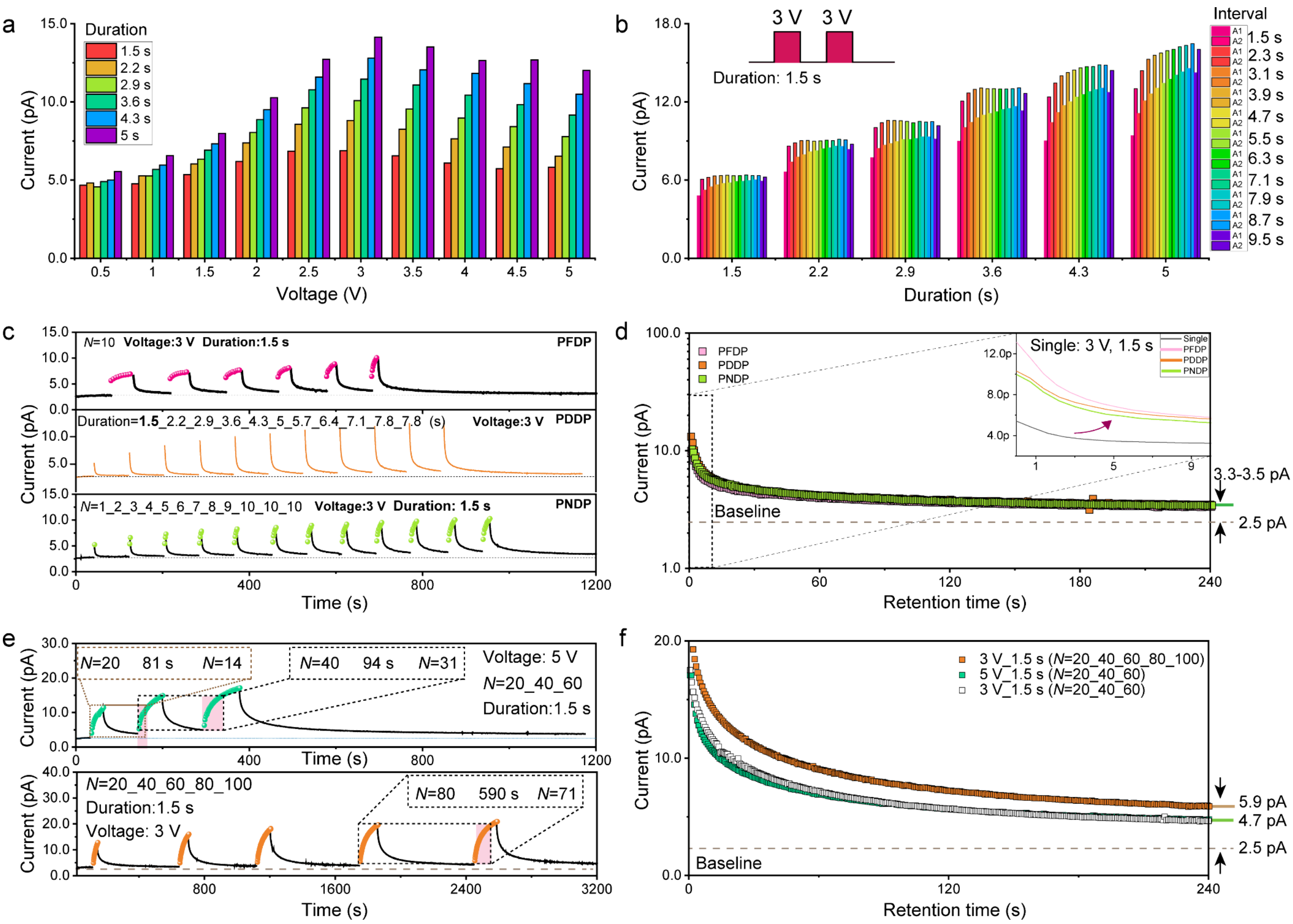

Figure 2. Plasticity in EC-MOF-L-ASs. a) Pulse-voltage-dependent plasticity (PVDP) changes in current peaks. b) Paired-pulse facilitation. c) Current changes and the corresponding d) current retention time curves under pulses of different frequencies, durations, and numbers (PFDP, PDDP, and PNDP). e) Current variation and the corresponding f) current-retention time curves after excitation using numerous pulses ($N \geq 20$). Inset: "Learning-experience" behavior under continuous pulse excitation.

*A*1 then *A*2) are generated in response (Figure 2b), with $A2 > A1$, which is called paired-pulse facilitation (PPF). The phenomenon occurs because the second pulse is applied before all ions have returned to their equilibrium after the end of the first pulse, so the total number of carriers at the interface after the second pulse is larger than after the first pulse.[54−56] This phenomenon is affected by the total excitation time, including the pulse width and the number of pulses. The effect of the second pulse on the interface ions over a brief interval (10 s) is quantified using the PPF index ($A2/A1 \times 100\%$; Supporting Information, Figure S9). The index has been shown to be correlated with pulse width.

To track changes in current retention following the cessation of pulse stimulation, the presynaptic pulse trains were arranged to differ in three ways (i.e., pulse frequency *f*, pulse number *N*, and pulse width; the corresponding forms of plasticity are defined as pulse-frequency-dependent plasticity PFDP, pulse-number-dependent plasticity PNDP and pulse-duration-dependent plasticity PDDP, respectively; Figure 2c). The parameters (τ_1 and τ_2) obtained under a double exponential function are considered to be the interaction strength of the ions and τ_2 is related to the number of pulses.[57] Here, the current decay trend is essentially the same at the end of the excitation of the three pulse sequences and the current remained >40% of its initial level after 4 min of "forgetting" (Figure 2d; Supporting Information, Figure S10); τ of the decay curves increased to 24 s. The learning-forgetting-relearning behavior (the Ebbinghaus forgetting curve) can be observed by counting the number of consecutive pulses (Figure 2e).[58] The current-decay curves were fairly consistent following excitation by two groups of pulse sequences with different amplitudes (3 and 5 V) but the same number (20, 40, 60); the current was 88% greater than the initial level after 4 min (Figure 2f). The retention curve of the current was further elevated and the current reached 236% of the initial value when the pulse number was increased to 100 (Supporting Information, Figure S11). The plasticity extension shown by EC-MOF-L-AS can be used as an emulation of classical conditioning learning (Supporting Information, Figure S12).[59−62] For instance, a powerful stimulus (i.e., food stimulus) with a bigger amplitude and wider duration is employed to deepen memory. When the food incentive is taken away for a while, the memory level steadily deteriorates, until the salivation response to the sound of the bell (i.e., relevance learning) fails.

For EC-MOF-N-AS, the responses of postsynaptic currents varying pulse frequencies demonstrate that pulse width induces greater changes in plasticity than pulse amplitude (Figure 3a). The current remained 120% above the baseline level for 4 min following the application of a longer-duration pulse (2.9 s),

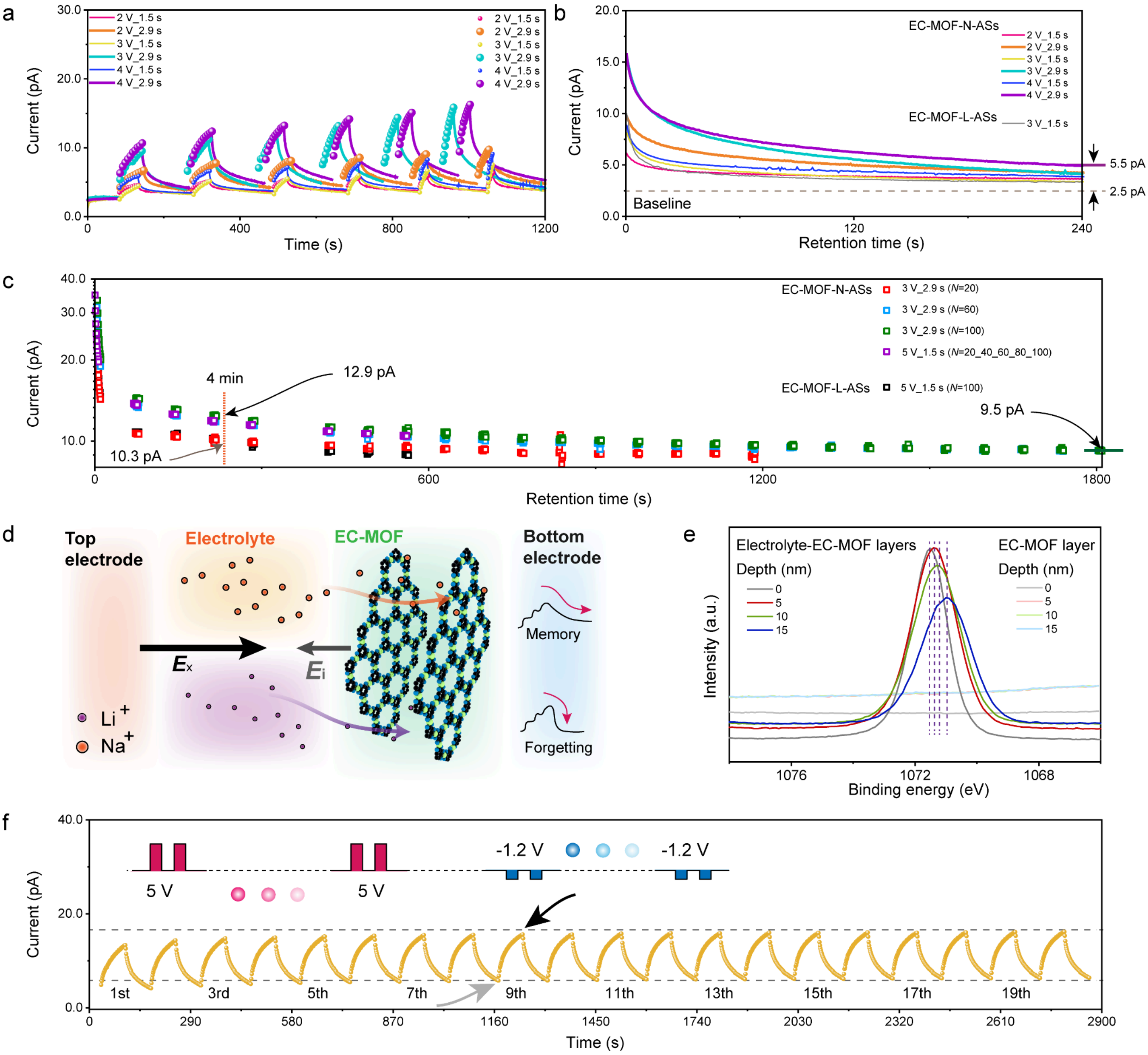

Figure 3. Plasticity in EC-MOF-N-ASs. a) Current changes and the corresponding b) current-retention-time curves under pulses of different frequencies. c) Current-retention time after excitation with $N \geq 20$ pulses. d) Interface mechanism of EC-MOF synaptic device. Lithium and sodium ions can migrate to the interface and then intercalate into EC-MOF under continuous spikes, demonstrating a plasticity change. e) High-resolution Na 1s spectra in three states (fresh film, tested film at 0, 5, 10, and 15 nm depth) of EC-MOF and electrolyte/EC-MOF film (removal of electrolyte layer after excitation). f) Cycles of potentiation and depression.

with a relaxation time exceeding 100 s (Figure 3b; Supporting Information, Figure S13). This retention level surpasses that observed under pulse excitation with a narrower width (1.5 s). However, the retention time curves of the two devices (EC-MOF-L-AS and EC-MOF-N-AS) were not noticeably shifted under the PFDP sequence with a 3 V amplitude. Enhanced current retention is achieved through the arrangement of multiple sets of pulse sequences (Figure 3c). When 100 consecutive pulses (3 V, 2.9 s) were applied, the current remained at 516% and 380% of its initial level after 4 and 30 min, respectively (Supporting Information, Figure S14). These results represent the highest retention levels achieved by the vertical electrolyte-type two terminal device, and is even comparable to some electrolyte-gate (such as metal ion polymer electrolytes and ionic liquids) three-terminal devices (Supporting Information, Table S1) as well as heterojunction memristors.[63,64] Alkali metal ions penetrate the pores of the EC-MOF under continuous pulse excitation, progressively increasing the internal electric field at the interface (Figure 3d). Ions can dope and dedope in EC-MOF due to the competition between the internal and exterior electric fields. A substantial concentration of sodium ions is present on the surface of the EC-MOF, as shown by high resolution XPS spectra at various depths (Figure 3e). The observed peak shifts with depth further confirm the doping process of sodium ions into the EC-MOF. Following an approximate 45 min period of forgetting, the learning-forgetting-relearning behavior was demonstrated (Supporting Information, Figure S15). Further-

https://doi.org/10.1021/acs.nanolett.4c04650
Nano Lett. 2024, 24, 15379−15387

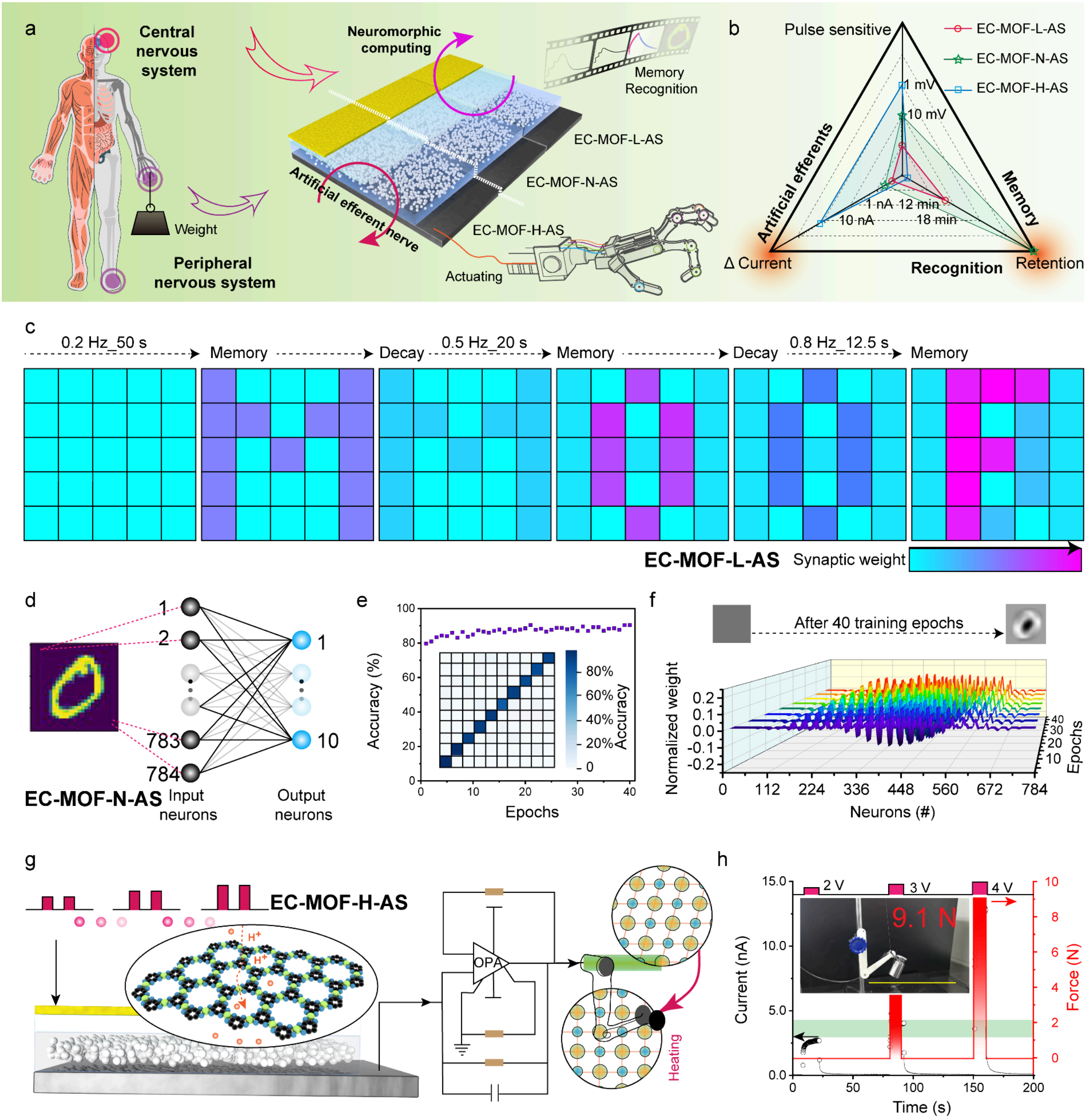

Figure 4. Demonstration of applications of plasticity changes in EC-MOF-ASs. a) Schematic diagram of the human central nervous system and peripheral nervous system and the development of three device applications. b) Radar maps of the performance of the three synaptic devices (EC-MOF-L-AS, EC-MOF-N-AS, and EC-MOF-H-AS). c) Real-time memory and forgetting of letters "M", "O", and "F". d) Neuron network structure for MNIST pattern recognition of EC-MOF-N-ASs. e) Estimated recognition rate for the MNIST patterns as a function of the training number. f) Weight changes for the MNIST patterns. g) Schematic illustration of an artificial efferent nerve, coupling EC-MOF-H-AS processing elements with artificial muscles, to transduce signals from receptors to motor neurons. h) Postsynaptic current of EC-MOF-H-ASs with corresponding output signal under successive pulses of different amplitudes. Inset: Digital image of the actuator according to postsynaptic current as triggered by pule with 4 V amplitude.

more, charge excitation at millivolt level pulses is attributable to the narrow bandgap properties of EC-MOF (~0.57 eV), achieved through incorporation of active *d*-electron transition metals, such as nickel, which facilitate enhanced orbital overlap. Consequently, the synaptic device exhibits response currents as low as subpicoamperes and power consumption at femtowatt levels (Supporting Information, Figure S16). Neuromorphic computing requires excellent current retention to achieve effective linear potentiation and depression.[65−69] For instance, the synaptic weights progressively rise and fall in a near-linear fashion while successively applying 50 positive and 50 negative pulses (Supporting Information, Figure S17). The dynamics of potentiation and depression showed progressive stabilization after several rounds of excitation with both positive and negative pulses (Figure 3f). The subnanometer pores of the EC-MOF inhibit the immediate release of ions under a constant, modest erasing voltage, allowing ions to enter the pores only during continuous positive pulse stimulation.

The human peripheral nervous system and central nervous system play crucial roles in information processing and memory storage, respectively.[70−72] This necessitates the development of devices capable of plasticity adjustments to facilitate the transition from short-term to long-term memory (Figure 4a). Synaptic devices exhibiting adjustable plasticity have potential applications in transient threshold switches (actuating), dynamic image refresh, and classification recognition (neuromorphic computing). The analysis indicates that EC-MOF-N-AS and EC-MOF-L-AS exhibit superior signal retention capabilities compared to EC-MOF-H-AS (Figure 4b). The former is suitable for neuromorphic computing applications, while the latter can be utilized in the development of sensitive threshold switches. Here, three applications, including image memory, pattern recognition, and signal transduction, were demonstrated using these electrolyte-type devices. By building an EC-MOF-L-AS array, a dynamic image refresh process is implemented (Figure 4c). A 25-pixel image created by a 5 × 5 array of EC-MOF-L-AS can be refreshed quickly due to the short-term plasticity of the synaptic unit when the letters "M", "O", and "F" are input into the array. Further pattern identification of handwritten digits from the Modified National Institute of Standards and Technology (MNIST) was accomplished using a single-layer artificial neural network (Figure 4d). The pattern recognition accuracy stabilized at 90.5% after 40 training epochs (Figure 4e). A clear figure can be observed from the mapped images of different training epochs (Figure 4f). Finally, an artificial efferent nerve was established by coupling highly responsive EC-MOF-H-AS (Supporting Information, Figure S18) with alloy fiber artificial muscles to demonstrate information transduction from electrical to mechanical signals (Figure 4g).[73] The output force of the actuator was 0, 3.5, and 9.1 N when three sets of continuous pulses were supplied to the fast-responding synaptic device (Supporting Information, Figure S19); this trend indicates that signal transduction had occurred in the artificial efferent neuron (Figure 4h; Supporting Information, Figure S20). Thus, the prospective uses of void-modulated materials in plasticity management have been confirmed as new applications of frameworks in electronic devices (Supporting Information, Table S2).

We successfully demonstrated synaptic devices that utilize redox-active EC-MOFs as ion-interactive layers. The interaction kinetics of various cations with the subnanometer pores of EC-MOF films were leveraged to implement versatile synaptic plasticity. Due to the open channels within the framework, the high-density redox centers in EC-MOF are fully accessible, significantly enhancing the long-term plasticity of these ionic/electronic hybrid synaptic devices. This advancement enables a voltage response reduction to as low as 10 mV, achieving power consumption as low as 1 femtowatt, and realizing the longest potentiation among two-terminal electrolyte-type artificial synapses. The successful demonstration of EC-MOF as a key component in neuromorphic devices and systems paves the way for the exploration of ultrasensitive and low-power brain-inspired electronics as well as artificial peripheral systems and neurorobotics.

■ ASSOCIATED CONTENT

Supporting Information

The Supporting Information is available free of charge at https://pubs.acs.org/doi/10.1021/acs.nanolett.4c04650.

> Experimental sections, TEM, AFM, and XPS for MOFs, $I-V$ curves and synaptic behaviors for MOF devices, digital images of the actuator, and performance comparisons (PDF)

■ AUTHOR INFORMATION

Corresponding Authors

Wentao Xu − *Institute of Photoelectronic Thin Film Devices and Technology, Nankai University, Tianjin 300350, PR China;* orcid.org/0000-0002-1054-6037; Email: wentao@nankai.edu.cn

Dawei Feng − *Materials Science and Engineering, University of Wisconsin-Madison, Madison, Wisconsin 53706, United States;* orcid.org/0000-0002-6285-850X; Email: dfeng23@wisc.edu

Authors

Huanhuan Wei − *Institute of Photoelectronic Thin Film Devices and Technology, Nankai University, Tianjin 300350, PR China; School of Materials Science and Engineering, Anhui University, Hefei 230601, PR China;* orcid.org/0000-0002-1306-5941

Jiaqi Liu − *Institute of Photoelectronic Thin Film Devices and Technology, Nankai University, Tianjin 300350, PR China*

Yao Ni − *Institute of Photoelectronic Thin Film Devices and Technology, Nankai University, Tianjin 300350, PR China*

Xuanxin Hu − *Materials Science and Engineering, University of Wisconsin-Madison, Madison, Wisconsin 53706, United States*

Xiuliang Lv − *Materials Science and Engineering, University of Wisconsin-Madison, Madison, Wisconsin 53706, United States;* orcid.org/0000-0002-7533-2718

Lu Yang − *Institute of Photoelectronic Thin Film Devices and Technology, Nankai University, Tianjin 300350, PR China*

Gang He − *School of Materials Science and Engineering, Anhui University, Hefei 230601, PR China*

Zhipeng Xu − *Institute of Photoelectronic Thin Film Devices and Technology, Nankai University, Tianjin 300350, PR China*

Jiangdong Gong − *Institute of Photoelectronic Thin Film Devices and Technology, Nankai University, Tianjin 300350, PR China*

Chengpeng Jiang − *Institute of Photoelectronic Thin Film Devices and Technology, Nankai University, Tianjin 300350, PR China;* orcid.org/0000-0003-4052-0804

Complete contact information is available at:
https://pubs.acs.org/10.1021/acs.nanolett.4c04650

Author Contributions

H.W., J.L., and Y.N. contributed equally. W.X. and D.F. conceived the original concept. W.X., D.F., and H.W. designed the experiments. H.W. fabricated the devices and performed electrical measurements. J.L designed the systems and prepared the circuits. Y.N. did the simulation. H.W., J.L., X.L., X.H., and L.Y. prepared electrolytes and MOFs. H.W., J.L., and Y.N. analyzed the data and H.W. wrote the manuscript. W.X. and D.F. supervised the research. All authors discussed the results and commented on the manuscript.

Notes

The authors declare no competing financial interest.

■ ACKNOWLEDGMENTS

This research is supported by National Science Fund for Distinguished Young Scholars of China (T2125005), National

Key R&D Program of China (2022YFE0198200, 2022YFA1204500, 2022YFA1204504), National Science Foundation of Tianjin (22JCYBJC01290), Key Project of Nature Science Foundation of Tianjin (22JCZDJC00120), NSF CAREER (award number DMR2143569), National Natural Science Foundation of China (52303306, 623B2055, and 62401536), Anhui Provincial Natural Science Foundation (2308085QE139), Guangdong Basic and Applied Basic Research Foundation (2023A1515110319), Scientific Research Project of Colleges and Universities in Anhui Province under Grant 2022AH050113, University Synergy Innovation Program of Anhui Province under Grant GXXT-2022-012, China Postdoctoral Science Foundation (2022M720184), Scientific Research Activities of Postdoctoral Researchers in Anhui Province (2023B667), and Jiangsu Funding Program for Excellent Postdoctoral Talent (345238). The authors would like to thank Xinpeng Sun from Xi'an Jiaotong University for the insightful discussion and assistance.

■ REFERENCES

(1) Kim, Y.; Chortos, A.; Xu, W.; Liu, Y.; Oh, J. Y.; Son, D.; Kang, J.; Foudeh, A. M.; Zhu, C.; Lee, Y.; et al. A bioinspired flexible organic artificial afferent nerve. *Science* **2018**, *360* (6392), 998−1003.

(2) Lee, Y.; Lee, T.-W. Organic Synapses for Neuromorphic Electronics: From Brain-Inspired Computing to Sensorimotor Nervetronics. *Acc. Chem. Res.* **2019**, *52* (4), 964−974.

(3) Choi, S.; Yang, J.; Wang, G. Emerging Memristive Artificial Synapses and Neurons for Energy-Efficient Neuromorphic Computing. *Adv. Mater.* **2020**, *32* (51), No. e2004659.

(4) Wang, M.; Luo, Y.; Wang, T.; Wan, C.; Pan, L.; Pan, S.; He, K.; Neo, A.; Chen, X. Artificial Skin Perception. *Adv. Mater.* **2021**, *33* (19), No. e2003014.

(5) Wang, W.; Jiang, Y.; Zhong, D.; Zhang, Z.; Choudhury, S.; Lai, J.-C.; Gong, H.; Niu, S.; Yan, X.; Zheng, Y.; Shih, C.-C.; Ning, R.; Lin, Q.; Li, D.; Kim, Y.-H.; Kim, J.; Wang, Y.-X.; Zhao, C.; Xu, C.; Ji, X.; Nishio, Y.; Lyu, H.; Tok, J. B. H.; Bao, Z. Neuromorphic sensorimotor loop embodied by monolithically integrated, low-voltage, soft e-skin. *Science* **2023**, *380* (6646), 735−742.

(6) Wang, T.; Wang, M.; Wang, J.; Yang, L.; Ren, X.; Song, G.; Chen, S.; Yuan, Y.; Liu, R.; Pan, L.; Li, Z.; Leow, W. R.; Luo, Y.; Ji, S.; Cui, Z.; He, K.; Zhang, F.; Lv, F.; Tian, Y.; Cai, K.; Yang, B.; Niu, J.; Zou, H.; Liu, S.; Xu, G.; Fan, X.; Hu, B.; Loh, X. J.; Wang, L.; Chen, X. A chemically mediated artificial neuron. *Nat. Electron.* **2022**, *5* (9), 586−595.

(7) Sun, L.; Du, Y.; Yu, H.; Wei, H.; Xu, W.; Xu, W. An Artificial Reflex Arc That Perceives Afferent Visual and Tactile Information and Controls Efferent Muscular Actions. *Research* **2022**, *2022*, 9851843.

(8) Zhu, L. Q.; Wan, C. J.; Guo, L. Q.; Shi, Y.; Wan, Q. Artificial synapse network on inorganic proton conductor for neuromorphic systems. *Nat. Commun.* **2014**, *5*, 3158.

(9) van de Burgt, Y.; Lubberman, E.; Fuller, E. J.; Keene, S. T.; Faria, G. C.; Agarwal, S.; Marinella, M. J.; Alec Talin, A.; Salleo, A. A non-volatile organic electrochemical device as a low-voltage artificial synapse for neuromorphic computing. *Nat. Mater.* **2017**, *16* (4), 414−418.

(10) Yang, J. T.; Ge, C.; Du, J. Y.; Huang, H. Y.; He, M.; Wang, C.; Lu, H. B.; Yang, G. Z.; Jin, K. J. Artificial Synapses Emulated by an Electrolyte-Gated Tungsten-Oxide Transistor. *Adv. Mater.* **2018**, *30*, No. e1801548.

(11) Wei, H.; Shi, R.; Sun, L.; Yu, H.; Gong, J.; Liu, C.; Xu, Z.; Ni, Y.; Xu, J.; Xu, W. Mimicking efferent nerves using a graphdiyne-based artificial synapse with multiple ion diffusion dynamics. *Nat. Commun.* **2021**, *12* (1), 1068.

(12) Liu, G.; Li, Q.; Shi, W.; Liu, Y.; Liu, K.; Yang, X.; Shao, M.; Guo, A.; Huang, X.; Zhang, F.; Zhao, Z.; Guo, Y.; Liu, Y. Ultralow-Power and Multisensory Artificial Synapse Based on Electrolyte-Gated Vertical Organic Transistors. *Adv. Funct. Mater.* **2022**, *32* (27), 2200959.

(13) van de Burgt, Y.; Melianas, A.; Keene, S. T.; Malliaras, G.; Salleo, A. Organic electronics for neuromorphic computing. *Nat. Electron.* **2018**, *1* (7), 386−397.

(14) Wan, C.; Cai, P.; Wang, M.; Qian, Y.; Huang, W.; Chen, X. Artificial Sensory Memory. *Adv. Mater.* **2020**, *32* (15), No. e1902434.

(15) Bu, X.; Xu, H.; Shang, D.; Li, Y.; Lv, H.; Liu, Q. Ion-Gated Transistor: An Enabler for Sensing and Computing Integration. *Adv. Intell. Syst.* **2020**, *2* (12), 2000156.

(16) He, Y.; Zhu, L.; Zhu, Y.; Chen, C.; Jiang, S.; Liu, R.; Shi, Y.; Wan, Q. Recent Progress on Emerging Transistor-Based Neuromorphic Devices. *Adv. Intell. Syst.* **2021**, *3* (7), 2000210.

(17) Shao, L.; Zhao, Y.; Liu, Y. Organic Synaptic Transistors: The Evolutionary Path from Memory Cells to the Application of Artificial Neural Networks. *Adv. Funct. Mater.* **2021**, *31* (28), 2101951.

(18) Xiang, L.; Liu, L.; Zhang, F.; Di, C. A.; Zhu, D. Ion-Gating Engineering of Organic Semiconductors toward Multifunctional Devices. *Adv. Funct. Mater.* **2021**, *31* (32), 2102149.

(19) He, Y.; Yang, Y.; Nie, S.; Liu, R.; Wan, Q. Electric-double-layer transistors for synaptic devices and neuromorphic systems. *J. Mater. Chem. C* **2018**, *6* (20), 5336−5352.

(20) Zhang, S.; Guo, K.; Sun, L.; Ni, Y.; Liu, L.; Xu, W.; Yang, L.; Xu, W. Selective Release of Different Neurotransmitters Emulated by a p-i-n Junction Synaptic Transistor for Environment-Responsive Action Control. *Adv. Mater.* **2021**, *33* (10), No. e2007350.

(21) Wei, H.; Han, H.; Guo, K.; Yu, H.; Gong, J.; Ma, M.; Ni, Y.; Feng, J.; Xu, Z.; Xu, W. Artificial synapses that exploit ionic modulation for perception and integration. *Mater. Today Phy* **2021**, *18*, 100329.

(22) Wei, H.; Ni, Y.; Sun, L.; Yu, H.; Gong, J.; Du, Y.; Ma, M.; Han, H.; Xu, W. Flexible electro-optical neuromorphic transistors with tunable synaptic plasticity and nociceptive behavior. *Nano Energy* **2021**, *81*, 105648.

(23) Wei, H.; Yu, H.; Gong, J.; Zhang, J.; Han, H.; Ma, M.; Ni, Y.; Du, Y.; Zhang, S.; Liu, L.; Xu, W. Lithium Ion Alloying-Type Artificial Synapses. *ACS Appl. Electron. Mater.* **2020**, *2* (2), 316−322.

(24) Wei, H.; Yu, H.; Gong, J.; Li, R.; Han, H.; Ma, M.; Guo, K.; Xu, W. A conversion-type electrochemical artificial synapse for plasticity modulation and dendritic application. *Mater. Chem. Front.* **2021**, *5* (2), 775−782.

(25) Seo, D.-G.; Lee, Y.; Go, G.-T.; Pei, M.; Jung, S.; Jeong, Y. H.; Lee, W.; Park, H.-L.; Kim, S.-W.; Yang, H.; Yang, C.; Lee, T.-W. Versatile neuromorphic electronics by modulating synaptic decay of single organic synaptic transistor: From artificial neural networks to neuro-prosthetics. *Nano Energy* **2019**, *65*, 104035.

(26) Go, G.-T.; Lee, Y.; Seo, D.-G.; Pei, M.; Lee, W.; Yang, H.; Lee, T.-W. Achieving Microstructure-Controlled Synaptic Plasticity and Long-Term Retention in Ion-Gel-Gated Organic Synaptic Transistors. *Adv. Intell. Syst.* **2020**, *2* (11), 2000012.

(27) Han, H.; Xu, Z.; Guo, K.; Ni, Y.; Ma, M.; Yu, H.; Wei, H.; Gong, J.; Zhang, S.; Xu, W. Tunable Synaptic Plasticity in Crystallized Conjugated Polymer Nanowire Artificial Synapses. *Adv. Intell. Syst.* **2020**, *2* (3), 1900176.

(28) Li, S.-L.; Xu, Q. Metal−organic frameworks as platforms for clean energy. *Energy Environ. Sci.* **2013**, *6* (6), 1656.

(29) Zhang, H.; Nai, J.; Yu, L.; Lou, X. W. Metal-Organic-Framework-Based Materials as Platforms for Renewable Energy and Environmental Applications. *Joule* **2017**, *1* (1), 77−107.

(30) Hou, C. C.; Xu, Q. Metal−Organic Frameworks for Energy. *Adv. Energy Mater.* **2019**, *9* (23), 1801307.

(31) Lu, X. F.; Fang, Y.; Luan, D.; Lou, X. W. D. Metal-Organic Frameworks Derived Functional Materials for Electrochemical Energy Storage and Conversion: A Mini Review. *Nano Lett.* **2021**, *21* (4), 1555−1565.

(32) Dhaka, S.; Kumar, R.; Deep, A.; Kurade, M. B.; Ji, S.-W.; Jeon, B.-H. Metal−organic frameworks (MOFs) for the removal of emerging contaminants from aquatic environments. *Coord. Chem. Rev.* **2019**, *380*, 330−352.

(33) Meteku, B. E.; Huang, J.; Zeng, J.; Subhan, F.; Feng, F.; Zhang, Y.; Qiu, Z.; Aslam, S.; Li, G.; Yan, Z. Magnetic metal−organic framework composites for environmental monitoring and remediation. *Coord. Chem. Rev.* **2020**, *413*, 213261.
(34) Zhang, S.; Wang, J.; Zhang, Y.; Ma, J.; Huang, L.; Yu, S.; Chen, L.; Song, G.; Qiu, M.; Wang, X. Applications of water-stable metal-organic frameworks in the removal of water pollutants: A review. *Environ. Pollut.* **2021**, *291*, 118076.
(35) McKinlay, A. C.; Morris, R. E.; Horcajada, P.; Ferey, G.; Gref, R.; Couvreur, P.; Serre, C. BioMOFs: metal-organic frameworks for biological and medical applications. *Angew. Chem., Int. Ed.* **2010**, *49* (36), 6260−6.
(36) Kumar, S.; Jain, S.; Nehra, M.; Dilbaghi, N.; Marrazza, G.; Kim, K.-H. Green synthesis of metal−organic frameworks: A state-of-the-art review of potential environmental and medical applications. *Coord. Chem. Rev.* **2020**, *420*, 213407.
(37) Zhou, Z.; Vazquez-Gonzalez, M.; Willner, I. Stimuli-responsive metal-organic framework nanoparticles for controlled drug delivery and medical applications. *Chem. Soc. Rev.* **2021**, *50* (7), 4541−4563.
(38) Liu, J.; Song, X.; Zhang, T.; Liu, S.; Wen, H.; Chen, L. 2D Conductive Metal−Organic Frameworks: An Emerging Platform for Electrochemical Energy Storage. *Angew. Chem., Int. Ed.* **2021**, *60* (11), 5612−5624.
(39) Xie, L. S.; Skorupskii, G.; Dinca, M. Electrically Conductive Metal-Organic Frameworks. *Chem. Rev.* **2020**, *120* (16), 8536−8580.
(40) Zhang, G.; Jin, L.; Zhang, R.; Bai, Y.; Zhu, R.; Pang, H. Recent advances in the development of electronically and ionically conductive metal-organic frameworks. *Coord. Chem. Rev.* **2021**, *439*, 213915.
(41) Luo, L. Architectures of neuronal circuits. *Science* **2021**, *373* (6559), No. eabg7285.
(42) Yang, Y. M.; Fedchyshyn, M. J.; Grande, G.; Aitoubah, J.; Tsang, C. W.; Xie, H.; Ackerley, C. A.; Trimble, W. S.; Wang, L. Y. Septins regulate developmental switching from microdomain to nanodomain coupling of Ca(2+) influx to neurotransmitter release at a central synapse. *Neuron* **2010**, *67* (1), 100−15.
(43) Wei, H.; Yu, H.; Gong, J.; Ma, M.; Han, H.; Ni, Y.; Zhang, S.; Xu, W. Redox MXene Artificial Synapse with Bidirectional Plasticity and Hypersensitive Responsibility. *Adv. Funct. Mater.* **2021**, *31* (1), 2007232.
(44) Gong, J.; Yu, H.; Wei, H.; Zheng, Y.; Yuan, C.; Ma, M.; Han, H.; Guo, K.; Xu, J.; Xu, W. An air-stable two-dimensional perovskite artificial synapse. *Semicond. Sci. Technol.* **2020**, *35* (10), 104001.
(45) Baek, J.-B.; Lah, M.; Mahmood, J.; Kim, D.; Jeon, I.-Y. Scalable Synthesis of Pure and Stable Hexaaminobenzene Trihydrochloride. *Synlett* **2013**, *24* (02), 246−248.
(46) Park, J.; Lee, M.; Feng, D.; Huang, Z.; Hinckley, A. C.; Yakovenko, A.; Zou, X.; Cui, Y.; Bao, Z. Stabilization of Hexaaminobenzene in a 2D Conductive Metal-Organic Framework for High Power Sodium Storage. *J. Am. Chem. Soc.* **2018**, *140* (32), 10315−10323.
(47) Feng, D.; Lei, T.; Lukatskaya, M. R.; Park, J.; Huang, Z.; Lee, M.; Shaw, L.; Chen, S.; Yakovenko, A. A.; Kulkarni, A.; Xiao, J.; Fredrickson, K.; Tok, J. B.; Zou, X.; Cui, Y.; Bao, Z. Robust and conductive two-dimensional metal−organic frameworks with exceptionally high volumetric and areal capacitance. *Nat. Energy* **2018**, *3* (1), 30−36.
(48) Tang, M.; Shen, H.; Sun, Q. Two-Dimensional Fe-Hexaaminobenzene Metal−Organic Frameworks as Promising CO_2 Catalysts with High Activity and Selectivity. *J. Phys. Chem. C* **2019**, *123* (43), 26460−26466.
(49) Park, J.; Hinckley, A. C.; Huang, Z.; Chen, G.; Yakovenko, A. A.; Zou, X.; Bao, Z. High Thermopower in a Zn-Based 3D Semiconductive Metal-Organic Framework. *J. Am. Chem. Soc.* **2020**, *142* (49), 20531−20535.
(50) Liu, C.; Gu, Y.; Liu, C.; Liu, S.; Li, X.; Ma, J.; Ding, M. Missing-Linker 2D Conductive Metal Organic Frameworks for Rapid Gas Detection. *ACS Sensors* **2021**, *6* (2), 429−438.
(51) Li, T.; He, C.; Zhang, W. Two-dimensional porous transition metal organic framework materials with strongly anchoring ability as lithium-sulfur cathode. *Energy Storage Mater.* **2020**, *25*, 866−875.
(52) Zeng, F.; Lu, S.; Li, S.; Li, X.; Pan, F. Frequency selectivity in pulse responses of Pt/poly(3-hexylthiophene-2,5-diyl)/polyethylene oxide + Li^+/Pt hetero-junction. *PLoS One* **2014**, *9* (9), No. e108316.
(53) Yan, X.; Zhao, J.; Liu, S.; Zhou, Z.; Liu, Q.; Chen, J.; Liu, X. Y. Memristor with Ag-Cluster-Doped TiO_2 Films as Artificial Synapse for Neuroinspired Computing. *Adv. Funct. Mater.* **2018**, *28* (1), 1705320.
(54) Xu, W.; Min, S.-Y.; Hwang, H.; Lee, T.-W. Organic core-sheath nanowire artificial synapses with femtojoule energy consumption. *Sci. Adv.* **2016**, *2* (6), No. e1501326.
(55) Yu, H.; Gong, J.; Wei, H.; Huang, W.; Xu, W. Mixed-halide perovskite for ultrasensitive two-terminal artificial synaptic devices. *Mater. Chem. Front.* **2019**, *3* (5), 941−947.
(56) Hu, L.; Li, L.; Chang, K. C.; Lin, X.; Huang, P.; Zhang, S. Ultrasensitive Freestanding and Mechanically Durable Artificial Synapse with Attojoule Power Based on Na-Salt Doped Polymer for Biocompatible Neuromorphic Interface. *Adv. Funct. Mater.* **2021**, *31* (42), 2106015.
(57) Zhang, Y.; Liu, L.; Tu, B.; Cui, B.; Guo, J.; Zhao, X.; Wang, J.; Yan, Y. An artificial synapse based on molecular junctions. *Nat. Commun.* **2023**, *14* (1), 247.
(58) Wang, W.; Gao, S.; Li, Y.; Yue, W.; Kan, H.; Zhang, C.; Lou, Z.; Wang, L.; Shen, G. Artificial Optoelectronic Synapses Based on TiN_xO_{2-x}/MoS_2 Heterojunction for Neuromorphic Computing and Visual System. *Adv. Funct. Mater.* **2021**, *31* (34), 2101201.
(59) Wu, C.; Kim, T. W.; Guo, T.; Li, F.; Lee, D. U.; Yang, J. J. Mimicking Classical Conditioning Based on a Single Flexible Memristor. *Adv. Mater.* **2017**, *29* (10), 1602890.
(60) Yu, F.; Zhu, L. Q.; Xiao, H.; Gao, W. T.; Guo, Y. B. Restickable Oxide Neuromorphic Transistors with Spike-Timing-Dependent Plasticity and Pavlovian Associative Learning Activities. *Adv. Funct. Mater.* **2018**, *28* (44), 1804025.
(61) Meng, J.-L.; Wang, T.-Y.; Chen, L.; Sun, Q.-Q.; Zhu, H.; Ji, L.; Ding, S.-J.; Bao, W.-Z.; Zhou, P.; Zhang, D. W. Energy-efficient flexible photoelectric device with 2D/0D hybrid structure for bio-inspired artificial heterosynapse application. *Nano Energy* **2021**, *83*, 105815.
(62) Wang, K.; Jia, Y.; Yan, X. A biomimetic afferent nervous system based on the flexible artificial synapse. *Nano Energy* **2022**, *100*, 107486.
(63) Li, R.; Wang, W.; Li, Y.; Gao, S.; Yue, W.; Shen, G. Multi-modulated optoelectronic memristor based on Ga_2O_3/MoS_2 hetero-junction for bionic synapses and artificial visual system. *Nano Energy* **2023**, *111*, 108398.
(64) Zhang, Z.-D.; Zhong, Y.-N.; Shen, C.; Huang, H.-T.; Lu, Z.-N.; Xu, J.-L.; Gao, X.; Wang, S.-D. A hybrid memristor with oxide-polymer heterojunction. *Appl. Phys. Lett.* **2022**, *121* (19), 191905.
(65) Sharbati, M. T.; Du, Y.; Torres, J.; Ardolino, N. D.; Yun, M.; Xiong, F. Low-Power, Electrochemically Tunable Graphene Synapses for Neuromorphic Computing. *Adv. Mater.* **2018**, *30*, No. e1802353.
(66) Li, J.; Ge, C.; Du, J.; Wang, C.; Yang, G.; Jin, K. Reproducible Ultrathin Ferroelectric Domain Switching for High-Performance Neuromorphic Computing. *Adv. Mater.* **2020**, *32* (7), No. e1905764.
(67) Wang, Y.; Zheng, Y.; Gao, J.; Jin, T.; Li, E.; Lian, X.; Pan, X.; Han, C.; Chen, H.; Chen, W. Band-tailored van der Waals heterostructure for multilevel memory and artificial synapse. *InfoMat* **2021**, *3* (8), 917−928.
(68) Tang, J.; He, C.; Tang, J.; Yue, K.; Zhang, Q.; Liu, Y.; Wang, Q.; Wang, S.; Li, N.; Shen, C.; Zhao, Y.; Liu, J.; Yuan, J.; Wei, Z.; Li, J.; Watanabe, K.; Taniguchi, T.; Shang, D.; Wang, S.; Yang, W.; Yang, R.; Shi, D.; Zhang, G. A Reliable All-2D Materials Artificial Synapse for High Energy-Efficient Neuromorphic Computing. *Adv. Funct. Mater.* **2021**, *31* (27), 2011083.
(69) Yang, S. T.; Li, X. Y.; Yu, T. L.; Wang, J.; Fang, H.; Nie, F.; He, B.; Zhao, L.; Lü, W. M.; Yan, S. S.; Nogaret, A.; Liu, G.; Zheng, L. M. High-Performance Neuromorphic Computing Based on Ferroelectric

Synapses with Excellent Conductance Linearity and Symmetry. *Adv. Funct. Mater.* **2022**, *32* (35), 2202366.
(70) Chen, Z.; Liang, Q.; Wei, Z.; Chen, X.; Shi, Q.; Yu, Z.; Sun, T. An overview of in vitro biological neural networks for robot intelligence. *Cyborg Bionic Syst.* **2023**, *4*, 0001.
(71) Wang, L.; Ma, L.; Yang, J.; Wu, J. Human somatosensory processing and artificial somatosensation. *Cyborg Bionic Syst.* **2021**, DOI: 10.34133/2021/9843259.
(72) Zhou, S.; Li, Y.; Wang, Q.; Lyu, Z. Integrated Actuation and Sensing: Toward Intelligent Soft Robots. *Cyborg Bionic Syst.* **2024**, *5*, 0105.
(73) Ni, Y.; Liu, L.; Liu, J.; Xu, W. A High-Strength Neuromuscular System That Implements Reflexes as Controlled by a Multiquadrant Artificial Efferent Nerve. *ACS Nano* **2022**, *16* (12), 20294−20304.